Supplementary Material

Near-infrared $^2E_g \rightarrow {}^4A_{2g}$ and visible LMCT luminescence from a molecular *bis*-(tris(carbene)borate) manganese(IV) complex

Valérie Baslon, Joe P. Harris, Christian Reber, Hannah E. Colmer, Timothy A. Jackson, Adam P. Forshaw, Jeremy M. Smith, R. Adam Kinney, and Joshua Telser

Table of contents

Figure S1. Luminescence spectra plotted with highest intensity matched S2

Figure S2. Variable-temperature Raman spectra S3

Figure S3. MCD and absorption spectra S4

Discussion of MCD spectra S4

Discussion of EPR spectra S6

Figure S4. X-band EPR spectra S9

Figure S5. Q-band EPR spectra S10

Electronic Structure Computations S11

Least-squares fit procedure for absorption and luminescence spectra S11

References S14

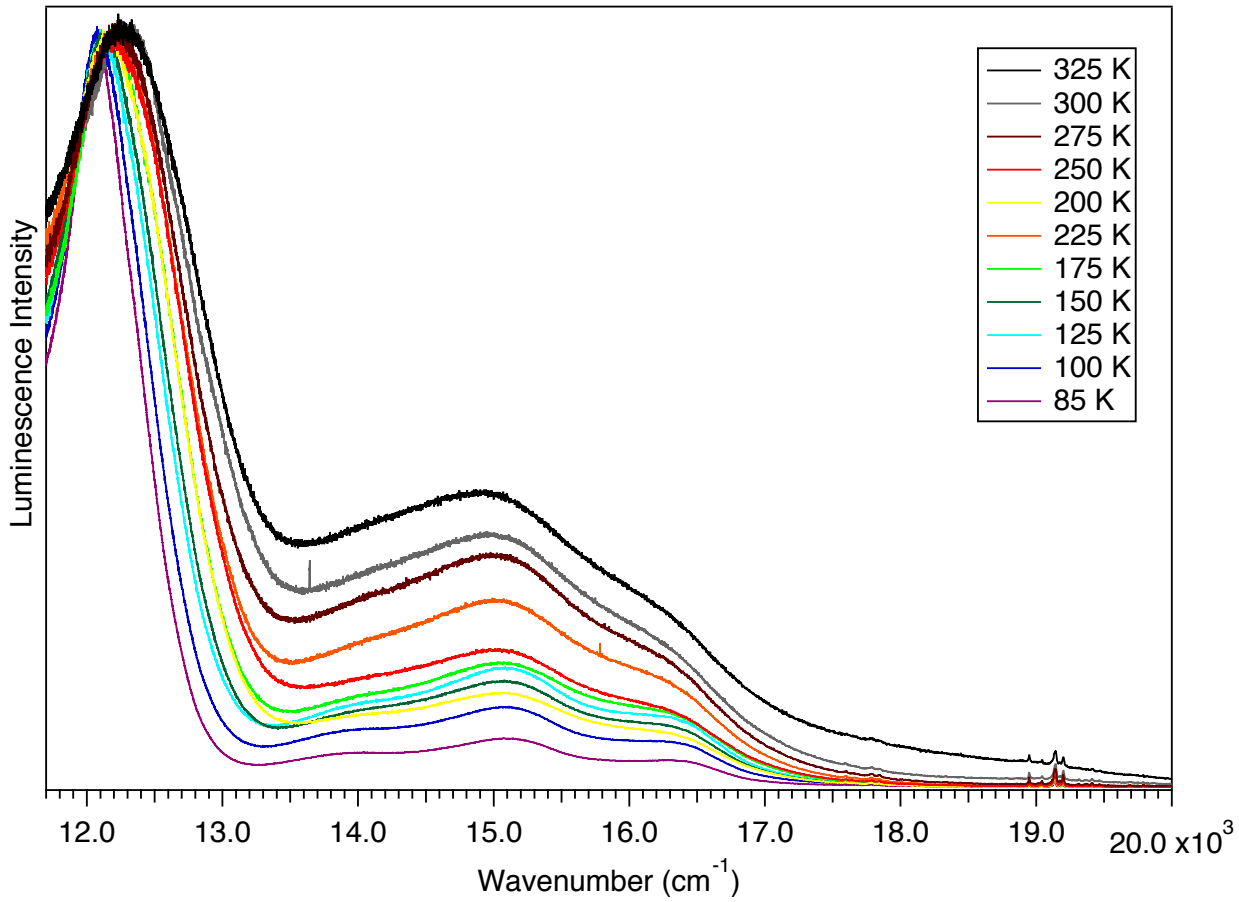

Figure S1. Luminescence spectra of solid $[\{PhB(MeIm)_3\}_2Mn](OTf)_2$ plotted with highest intensity matched. Excitation wavelength is 488 nm.

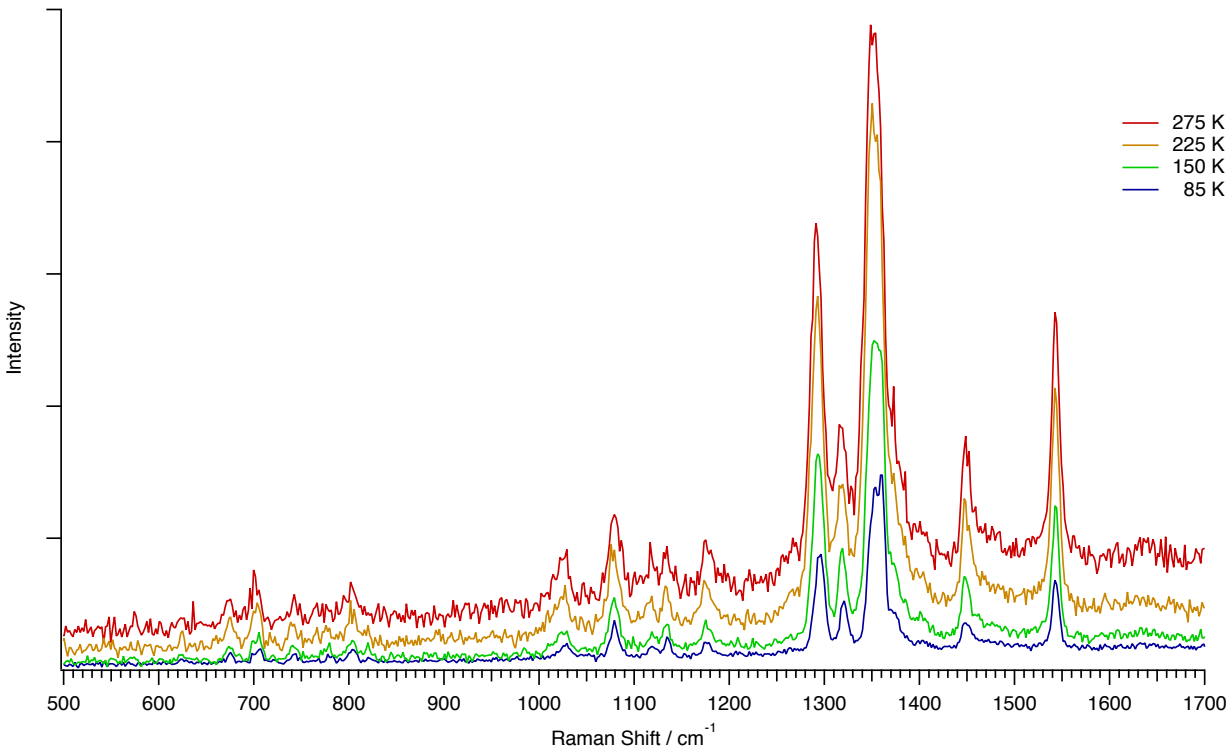

Figure S2. Raman spectra of $[\{PhB(MeIm)_3\}_2Mn](OTf)_2$ at variable temperature. The excitation wavelength is 488 nm. Raman shifts lower than 500 cm^{-1} are not accessible due to instrumental limitations.

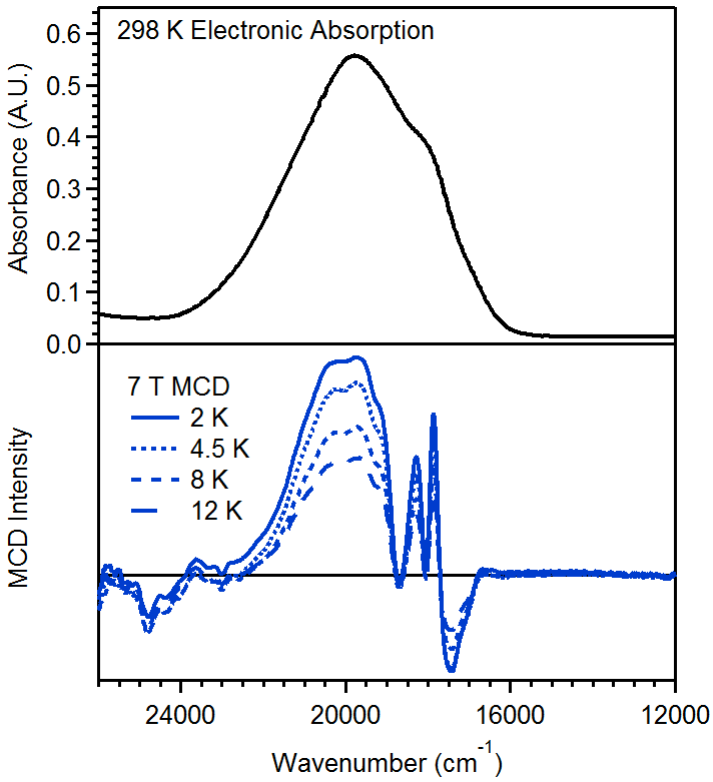

Figure S3. Top: Electronic absorption spectrum of 0.1 mM $[Mn^{IV}(PhB(MeIm)_3)_2]^{2+}$ in butyronitrile. Bottom: Variable-temperature, 7 T MCD spectrum of a mull sample of $[Mn^{IV}(PhB(MeIm)_3)_2](OTf)_2$.

Electronic Absorption and MCD Data for $[Mn^{IV}(PhB(MeIm)_3)_2]^{2+}$.

MCD Experiments. MCD data for $[Mn^{IV}(PhB(MeIm)_3)_2]^{2+}$ were collected for a thin mull sample of solid $[Mn^{IV}(PhB(MeIm)_3)_2](OTf)_2$ dispersed in Fluorolube. Data were collected between 2 K and 12 K and fields of 1 T to 7 T. Background effects unassociated with the MCD signal were minimized by taking the difference between magnetic field aligned parallel and antiparallel with the axis of light propagation. MCD data were collected using a Jasco J-815 spectropolarimeter interfaced with an Oxford Instruments SM-4000-8 magnetocryostat.

The electronic absorption spectrum of $[Mn^{IV}(PhB(MeIm)_3)_2]^{2+}$ (0.1 mM solution in

butyronitrile; see Figure S3, top) reveals a broad maximum near 19800 cm^{-1} (500 nm) with a shoulder on the lower-energy side (near 17950 cm^{-1} or 557 nm). At this concentration, the electronic absorption spectrum shows no appreciable features between 9000 cm^{-1} and 15000 cm^{-1}. At higher energies, the onset of more intense absorption features begins at ~28000 cm^{-1}. To gain additional insights into the electronic transitions of $[Mn^{IV}(PhB(MeIm)_3)_2]^{2+}$, low-temperature MCD data were collected on a mull sample of the triflate salt dispersed in fluorolube. High-quality data were only able to be collected below 24000 cm^{-1}. At higher energies, the intense absorption of the sample degraded the MCD signal considerably. Nonetheless, MCD data collected in this limited energy range reveal insights into the electronic structure of $[Mn^{IV}(PhB(MeIm)_3)_2]^{2+}$. In contrast to the rather uninformative electronic absorption spectrum, the low-temperature MCD spectrum of $[Mn^{IV}(PhB(MeIm)_3)_2]^{2+}$ shows fairly rich structure between 16000 cm^{-1} and 23000 cm^{-1} (Figure S3, bottom). The MCD spectrum contains a set of negatively- and positively-signed features at 17440 (-) cm^{-1}, 17870 (+) cm^{-1}, and 18295 (+) cm^{-1} that correspond to the shoulder in the electronic absorption spectrum. In addition, a broader, positive MCD signal is observed at 19800 cm^{-1}, which corresponds with the major electronic absorption signal of $[Mn^{IV}(PhB(MeIm)_3)_2]^{2+}$. All these MCD signals show an increase in intensity with decreasing temperature. This is referred to as *C*-term behavior[1-2] and is expected for a paramagnetic species such as $[Mn^{IV}(PhB(MeIm)_3)_2]^{2+}$.

The lower-energy bands between 17000 cm^{-1} and 18000 cm^{-1} display full-width at half-maximum (FWHM) values ranging from 544 cm^{-1} to 185 cm^{-1}. These widths are narrower than expected for either ligand-to-metal charge transfer (LMCT) or spin-allowed ligand-field transitions. In addition, the negatively-signed feature has an asymmetric band-shape. In comparison, the higher-energy MCD band centered at 19800 cm^{-1} has a FWHM of 2322 cm^{-1},

which is perfectly compatible with an LMCT transition. The unusual widths of the lower-energy bands could either be attributed to vibronic fine structure of an LMCT transition or the interaction of an LMCT excited state with spin-forbidden ligand-field excited states. The spacing of the narrow, low-energy bands is ~400 cm^{-1}, which could correspond to metal-ligand vibrational modes. In addition, the broader MCD band at 19800 cm^{-1} appears to show less resolved fine structure, with a spacing of ~500 cm^{-1}. Thus, the collective data tend to suggest the unusual lineshape is due, at least in part, to vibronic coupling. However, it is certainly possible that spin-forbidden excited states present in this energy region could contribute to the MCD dispersion of the lower-energy transitions.

EPR Data for $[Mn^{IV}(PhB(MeIm)_3)_2]^{2+}$.

EPR Experiments. Frozen solution (1:1 v/v acetonitrile/toluene) spectra were recorded for $[Mn^{IV}(PhB(MeIm)_3)_2]^{2+}$ using several spectrometers: a modified Varian E4 X-band spectrometer equipped with a liquid nitrogen finger dewar, a modified Bruker X-band ESP 300 spectrometer equipped with an Oxford Instruments ESR 910 continuous He flow cryostat, and a CW 35 GHz (Q-band) modified Varian E-109 EPR/ENDOR spectrometer, which is described in detail elsewhere.[3] All CW Q-band EPR spectra were recorded at 2 K in dispersion mode under "rapid passage" conditions,[4] which gives an absorption line shape.

Only a very weak signal (not shown) was observed for $[Mn^{IV}(PhB(MeIm)_3)_2]^{2+}$ at X-band (9.2 GHz) and 77 K. EPR spectra of Mn(IV) complexes can be observable at 77 K or higher temperatures,[5,6] however, lower temperatures ($T \leq 20$ K) are more commonly employed.[7] Consistent with that finding, EPR signals were readily observed for $[Mn^{IV}(PhB(MeIm)_3)_2]^{2+}$ at X-band 4 K and 10 K, shown in Figure S4. The spectrum recorded at 4 K was notably more

intense than that at 10 K, under otherwise the same experimental conditions. There is a prominent perpendicular feature at $g = 4.36$ and a weaker, low field feature at $g = 9.8$, along with a parallel feature that is barely within the magnetic field range, and is located at $g \approx 1.34$. We note that no resolved ^{55}Mn (I = 5/2, 100%) hyperfine coupling was observed here, nor was it observed for the tris(pyrazolyl)borate complex, $[Tp^*_2Mn]^{2+}$,[5] or another Mn(IV) complex.[6] Such an EPR spectrum results from a spin quartet where the zero-field splitting (ZFS) is roughly comparable to the microwave energy.[8] Spectra of this type have been reported for other Mn(IV) complexes.[6,7] In contrast, the X-band EPR spectrum for the most closely related species, namely $[Tp^*_2Mn]^{2+}$, recorded at 100 K in acetonitrile solution, is distinctly different.[5] It shows a spectrum typical for the spin quartet situation where the ZFS is positive and much greater than the microwave quantum (~0.3 cm^{-1}), so that only well-defined $g_\perp \approx 4$ and $g_\parallel \approx 2.0$ features are seen.[8] Simulation of the X-band spectrum for $[Mn^{IV}(PhB(MeIm)_3)_2]^{2+}$ (Figure S4) suggests that the axial ZFS, $|D| = 0.22$ cm^{-1}, with a slight rhombic contribution ($|E/D| = 0.1$).

To confirm that the features seen at X-band were due to ZFS of a spin quartet, Q-band spectra were also recorded. A representative spectrum is shown in Figure S5. Note that under these experimental conditions, the spectrum appears as an absorption lineshape; for ease of comparison with conventional EPR (as in Figure S4), a digital derivative is also shown. The simulated Q-band spectrum uses identical spin Hamiltonian parameters as the X-band simulation. There is a reasonable match at both frequencies between experiment and simulation. Accurate determination of ZFS in such a complex, as well as in $[Tp^*_2]Mn]^{2+}$ where the ZFS is larger, would require use of high-field and -frequency EPR (HFEPR), as has been successfully employed by by Zlatar et al. on a wide series of six-coordinate Mn(IV) complexes.[9] We can, however, make use of this extensive study and see that the D value estimated for the present

complex is in line, and perhaps on the low side, for six-coordinate Mn(IV) complexes. The overall conclusion from the EPR studies, of relevance for the luminescence investigation, is that $[Mn^{IV}(PhB(MeIm)_3)_2]^{2+}$ exhibits a ground state that is unremarkable for a six-coordinate Mn(IV) complex. That the ZFS is likely smaller in magnitude than that for its closest relative, namely $[Tp^*_2Mn]^{2+}$, may be qualitatively a function of the greater quenching of spin-orbit coupling in the more covalent imidazolyl (carbene) complex versus the pyrazolyl complex. This finding is in line with the low β value derived from the luminescence spectroscopy.

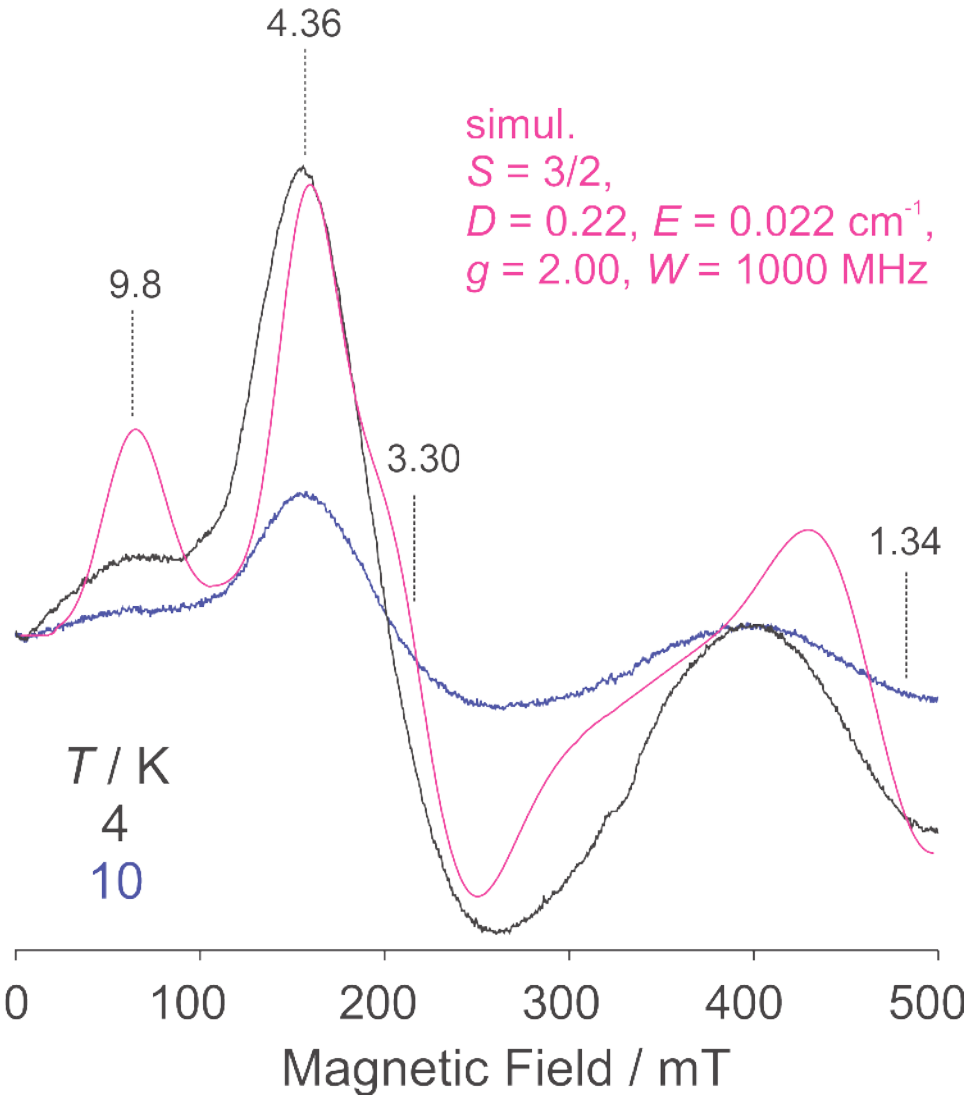

Figure S4. X-band EPR spectra recorded for $[Mn^{IV}(PhB(MeIm)_3)_2]^{2+}$ at 4 K (black trace) and 10 K (blue trace) with a simulation (magenta trace). Experimental parameters: microwave frequency, 9.3725 GHz; microwave power, 0.2 mW; 100 kHz magnetic field modulation amplitude, 0.4 mT; time constant, 40 ms; scan time, 150 s. Simulation parameters: S = 3/2, D = 0.22 cm^{-1}, E = 0.022 cm^{-1}, Gaussian single-crystal linewidth (HWHM) 1000 MHz.

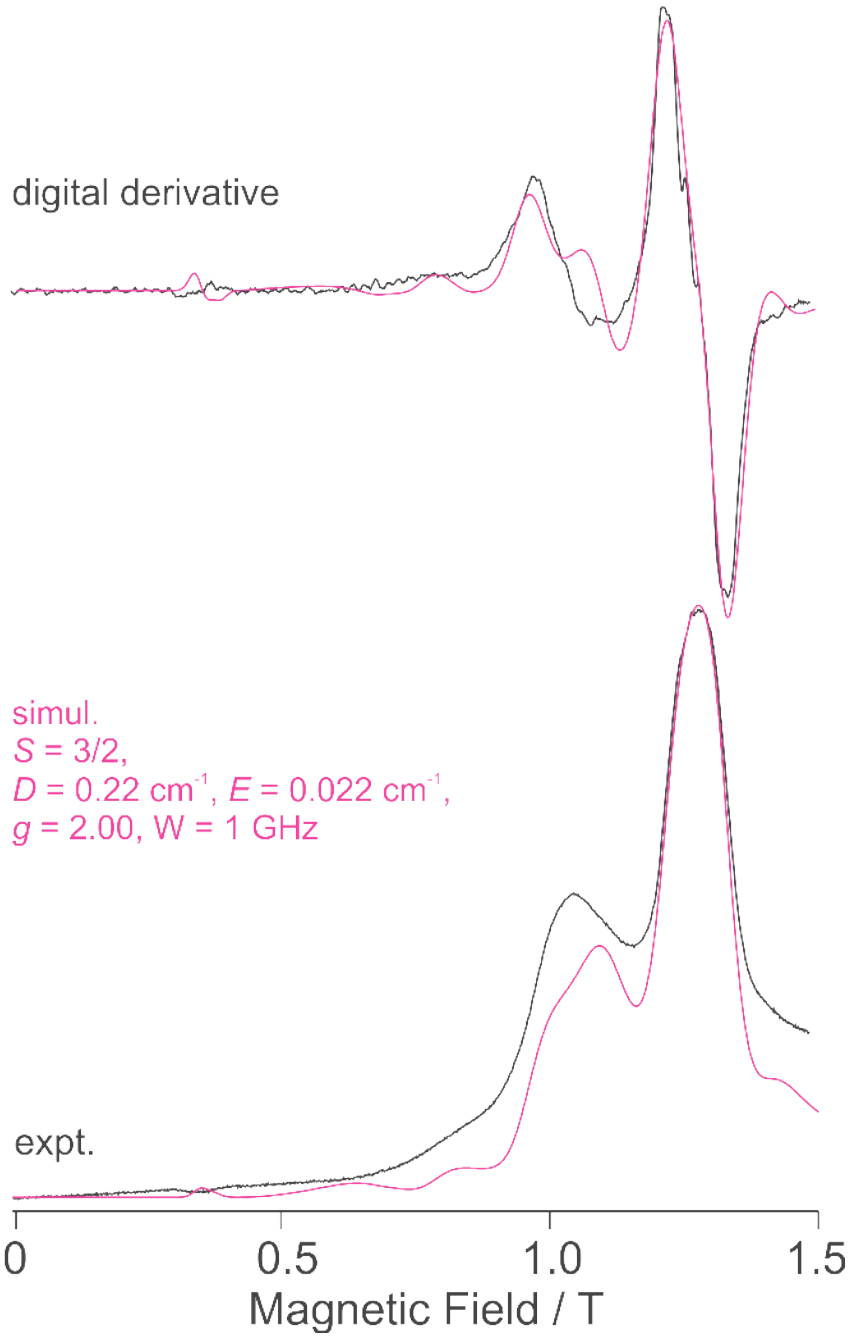

Figure S5. Q-band EPR spectrum recorded for $[Mn^{IV}(PhB(MeIm)_3)_2]^{2+}$ at 2 K (black trace) with a simulation (magenta trace). Both the experimental absorption shape spectrum and digital first derivative spectrum are shown for each. Experimental parameters: microwave frequency, 35.2764 GHz; microwave power, 2 mW; 100 kHz magnetic field modulation amplitude, 0.1 mT; time constant, 32 ms; scan time, 120 s. Simulation parameters: S = 3/2, D = 0.22 cm^{-1}, E = 0.022 cm^{-1}, Gaussian single-crystal linewidth (HWHM) 1000 MHz.

Electronic Structure Computations. All electronic structure computations were performed using the ORCA program.[10] Computations for $[(PhB(MeIm)_3)_2Mn]^{2+}$ utilized atomic coordinates from the previously reported X-ray diffraction structure.[11] All calculations were tightly converged to the $S = 3/2$ ground state and performed at the spin unrestricted level. The positions of the hydrogen atoms, which are not as well-defined crystallographically as those of the heavy atoms, were optimized at the DFT level using the BP functional[12-13] with TZVP (Mn, N, and coordinating C atoms) and SVP (H and non-coordinating C atoms) basis sets.[14] Ground-state zero-field splitting parameters were calculated using the coupled-perturbed DFT approach,[15] which employed the hybrid B3LYP/G functional[16-18] and the same basis sets employed in the geometry optimization calculation. These calculations yielded $D = 0.14$ cm^{-1} and $E/D = 0.33$. These values are compatible with the EPR analysis, especially given that the zero-field splitting in a spin quartet (i.e., the $M_S = |\pm 1/2 - \pm 3/2|$ energy separation) is given by $\Delta = 2(D^2 + 3E^2)^{1/2}$, so that $\Delta = 0.44$ cm^{-1} from EPR and 0.32 cm^{-1} computationally. We note that, although the CP-DFT approach is often of dubious quality for treating transition-metal zero-field splitting,[19-20] this method performs respectably for mononuclear Mn(IV) centers.[9,21-22] The TD-DFT calculations performed for the Mn(IV) complex predict three intense LMCT transitions in the visible region, a result consistent with the MCD data. Because of the large size of the system, the calculations were limited to only thirty excited states, the highest of which lies near 31 000 cm^{-1}. All excited states are charge-transfer in nature. Thus, the TD-DFT method predicts the Mn(IV) ligand-field transitions to lie above 31 000 cm^{-1}.

Least-squares fit procedure for absorption and luminescence spectra. The spectra of the weaker features at ~500 nm in absorption and ~650 nm in luminescence were fitted

simultaneously, using the wavepacket-propagation model outlined in the manuscript. The optimisation was performed using the implementation of the Levenberg-Marquadt non-linear least squares fitting procedure included in the SciPy package, leastsq, which is equivalent to the MINPACK functions lmdif and lmder.

Two extra, non-physical parameters needed to be included in each calculation in order for the fitting procedure to work correctly. The first of these is a simple y-scaling factor. The other is a y-shift parameter, required to compensate for uncertainties in the experimental baselines of the two spectra being fitted. Without these two parameters, the fitting procedure fails completely, even when supplied with initial parameters very close to convergence. Inclusion of the shift resulted in a small negative value, which did not exceed 0.2 for emission, and was much lower for absorption.

Initial parameters were decided upon by approximate manual optimisation, using the visual quality of the fit to determine appropriate values. When starting values were far from suitable, the optimisation procedure would struggle to find a reasonable region of parameter space, presumably due to the high-dimensionality of the problem. The fitting procedure was also seen to suffer major difficulties when the experimental data was not normalised prior to fitting; this treatment also has the added benefit of roughly normalising the range of expected residuals for both absorption and luminescence fits, applying close-to-equal weighting to both spectra in the optimisation procedure.

The spectral range of the fit also had to be restricted, since the spectra show additional structure outside of the region of interest which is not accounted for by the model. This point is illustrated well by the luminescence spectrum, which features a very sharp increase in intensity

to lower energy, and a very long tail of gradually decreasing intensity with Raman features on top to higher energy, neither of which are explicitly included in the model used for the calculations. Optimised parameters were seen to vary only insignificantly with modest changes to the imposed boundaries, with similarly insignificant variations in the magnitude of χ^2, nor did it affect the overall shape of the fit, with a clear correspondence between the form of the calculated spectrum and the experimental spectrum being evident throughout.

Parameters:

Emission bounds: 13 300 - 16 900 cm^{-1}

Absorption bounds: 16 700 - 24 500 cm^{-1}

Emission scaling factor = 1.464

Absorption scaling factor = 0.245

Emission y shift = -0.197

Absorption y shift = -0.064

References

(1) Neese, F.; Solomon, E. I. *Inorg. Chem.* **1999**, *38*, 1847-1865.
(2) Piepho, S. B.; Schatz, P. N., *Group Theory in Spectroscopy with Applications to Magnetic Circular Dichroism*. Wiley: New York, 1983.
(3) Werst, M. M.; Davoust, C. E.; Hoffman, B. M. *J. Am. Chem. Soc.* **1991**, *113*, 1533-1538.
(4) Mailer, C.; Taylor, C. P. S. *Biochimica et Biophysica Acta* **1973**, *322*, 195-203.
(5) Chan, M. K.; Armstrong, W. H. *Inorg. Chem.* **1989**, *28*, 3777-3779.
(6) Duboc, C.; Collomb, M.-N. *Chem. Commun.* **2009**, 2715-2717.
(7) Duboc, C. *Chem. Soc. Rev.* **2016**.
(8) Weltner, W., Jr., *Magnetic Atoms and Molecules*. Dover Publications, Inc.: Mineola, NY, 1983; p 156-219.
(9) Zlatar, M.; Gruden, M.; Vassilyeva, O. Y.; Buvaylo, E. A.; Ponomarev, A. N.; Zvyagin, S. A.; Wosnitza, J.; Krzystek, J.; Garcia-Fernandez, P.; Duboc, C. *Inorg. Chem.* **2016**, *55*, 1192-1201.
(10) Neese, F., *Wiley Interdisciplinary Reviews: Computational Molecular Science* **2012**, *2*, 73-78.
(11) Forshaw, A. P.; Bontchev, R. P.; Smith, J. M., *Inorg. Chem.* **2007**, *46*, 3792-3794.
(12) Becke, A. D., *J. Chem. Phys.* **1986**, *84*, 4524-4529.
(13) Perdew, J. P., *Physical Review B* **1986**, *33*, 8822-8824.
(14) Schäfer, A.; Huber, C.; Ahlrichs, R., *J. Chem. Phys.* **1994**, *100*, 5829-5835.
(15) Neese, F., *J. Chem. Phys.* **2007**, *127*, 164112-164119.
(16) Becke, A. D., *J. Chem. Phys.* **1993**, *98*, 1372-1377.
(17) Becke, A. D., *J. Chem. Phys.* **1993**, *98*, 5648-5652.
(18) Lee, C.; Yang, W.; Parr, R. G., *Phys. Rev. B* **1988**, *37*, 785-789.
(19) Atanasov, M.; Aravena, D.; Suturina, E.; Bill, E.; Maganas, D.; Neese, F., *Coord. Chem. Rev.* **2015**, *289–290*, 177-214.
(20) Atanasov, M.; Comba, P.; Helmle, S.; Müller, D.; Neese, F., *Inorg. Chem.* **2012**, *51*, 12324-12335.
(21) Leto, D. F.; Massie, A. A.; Colmer, H. E.; Jackson, T. A., *Inorg. Chem.* **2016**, *55*, 3272-3282.
(22) Gupta, R.; Taguchi, T.; Borovik, A. S.; Hendrich, M. P. *Inorg. Chem.* **2013**, *52*, 12568-12575.